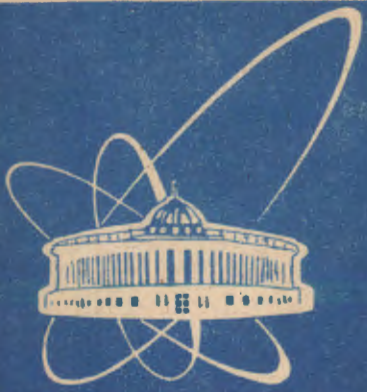

ОБЪЕДИНЕННЫЙ
ИНСТИТУТ
ЯДЕРНЫХ
ИССЛЕДОВАНИЙ

Дубна

E14-96-185

K.Wieteska[1], W.Wierzchowski [2], W.Graeff [3]

LATTICE DEFORMATION STUDIES IN HIGH ENERGY IONS IMPLANTED SILICON BY MEANS OF VARIOUS X-RAY METHODS

To be presented at the Third Radiation Conference,
November 13—17, 1996, Egypt

[1]Institute of Atomic Energy, Otwock-Swierk, Poland
[2]Institute of Electronic Materials Technology, Warsaw, Poland
[3]HASYLAB at DESY, Hamburg, Germany

1996

Introduction

In recent years ion implantation was introduced into technology of electronic devices. Many physical phenomena in the process of implantation are yet not well know and can be studied with X-ray diffraction methods, which were applied to the implanted layers in a number of papers [1-4].

In the present paper we confront results obtained with different X-ray methods in silicon implanted with light particles of high energies: 4.8 MeV α-particles and 1 and 1.6 MeV protons. These results seem be interesting in aspect of diffraction phenomena and new method of experiment. On the other hand in actual case many original diffraction phenomena were well explained basing on the theoretical prediction of the distribution of ions and related defects. Some of the confronted results were published in our former papers [5-7].

Good theoretical approximations of rocking curves and topographical contrast were obtained by numerical integration of Takagi-Taupin equations taking into account a vertical incoherence coming from the mutual displacement of the lattice in the substrate and the shot-through layer.

1. Experimental

The experiments were performed on (111) oriented silicon crystals implanted with 4.8 MeV α -particles and 1 and 1.6 MeV protons. The ion doses were 1×10^{16} cm^{-2} for α-particles and 1×10^{17} cm^{-2} for protons. In the most cases the significantly thick substrates in the range 1.5 - 6 mm were used and the radius of curvature was greater than 1000 m. The 1 and 1.6 MeV protons were implanted in two neighbouring regions of the same sample.

The samples were studied with different topographic methods and rocking curve measurements. Part of the experiments were realized using synchrotron source of X-rays.

The important results were obtained with the use of the back-reflection synchrotron section topography. The section experiments were performed using white beam X-ray radiation from the DORIS III storage ring operating with the energy of 4.455 GeV. The wave front of the beam in the section experiments was limited by 5 μm slit. The angle of incidence was chosen to be equal to 8.5°. Each exposure revealed a number of reflections which were indexed using numerical program.

The use of synchrotron radiation multicrystal arrangement enabled systematic recording of rocking curves from very small fragments of implanted region.

2. Numerical calculation

The rocking curves were obtained from the form of Takagi-Taupin equations assuming the solution dependent only on the vertical coordinate z:

$$\gamma_0 \frac{i}{\pi k}\frac{dD_0}{dz} = \chi_0 D_0 + C\chi_{\bar{h}} D_h, \qquad \gamma_h \frac{i}{\pi k}\frac{D_h}{dz} = C\chi_h D_0 - \alpha_h D_h \tag{1}$$

The equations are integrated towards the surface starting from the top regions of the substrate with the values corresponding to the analytical solution in the semi-infinite crystal [8].

A modification of the program was applied for simulation of the fringe pattern observed in the double-crystal topographs. We assumed here that the lateral variation of lattice deformation is slow enough so locally we may still use equations (1). The beam divergence was taken into account by adding appropriate number of values calculated for different angle of incidence.

The simulations of back-reflection section images were performed using fine constant step close to 0.5 μm and the normal form of Takagi Taupin equations:

$$\frac{i}{\pi k}\frac{\partial D_0}{\partial s_0} = \chi_0 D_0 + C\chi_{\bar{h}} D_h, \qquad \frac{i}{\pi k}\frac{\partial D_h}{\partial s_h} = C\chi_h D_0 - \alpha_h D_h \tag{2}$$

A good correspondence between the theoretical and experimental curves was achieved approximating lattice parameter profile by a distribution of vacancies and interstitial computed using the TRIM-85 program published by Biersack and Ziegler [9].

The essential for obtaining a good approximation of fringes in back-reflection double-crystal topograph and in the back-reflection section topography is taking into account the mutual displacement of the lattice of the shot-through layer with respect to the bulk crystal being the integral of the lattice parameter change. That was realized multiplying χ_h and $\chi_{\bar{h}}$ by a factor $\exp[\pm 2\pi i f(z)]$ where z is the co-ordinate perpendicular to the surface. The function $f(z)$ is proportional to the integral of lattice parameter change profile:

$$f(z) = p\int_0^z \Delta a(t)\,dt \tag{3}$$

where

$$\Delta a(z) = a(z) - a_s \tag{4}$$

means the difference between the lattice parameter at the depth z and its value in the substrate a_s. It may be easily found that at assumed absence of plastic deformation and that the planes perpendicular to the surface are straight.

$$p = \frac{\cos\varphi M}{a_s} \tag{5}$$

where φ is the inclination of the reflecting planes to the surface and M is expressed by Poisson coefficient ν as in [10]

$$M = \frac{1+\nu}{1-\nu} \tag{6}$$

3. Results and discussion

The rocking curves recorded using synchrotron multicrystal arrangement and small diameter of the probe beam provided a very good resolution of the subsidiary maxima as may be seen in Fig. 1. The curve *a* corresponds to lower dose of 1 MeV protons than curve *b*. The higher dose causes larger separation between the main peaks due to the substrate and top region of the shot-through layer. The subsidiary maxima are much more visible at higher dose due to the stronger lattice parameter gradient.

The theoretical curves reproducing the character of experimental ones were obtained by numerical integration of the Takagi-Taupin equations assuming the lattice depth distribution profile proportional to the vacancy-interstitial distribution profiles produced by Biersack-Ziegler program TRIM-85, see Fig. 2. It may be expected that both vacancies and interstitials should result the effective increase of lattice parameter. The reasonable angular positions of subsidiary maxima were obtained assuming validity of eq. (5). The theoretical curves are shown in Fig. 3.

It is expected that a good approximation of lattice parameter profiles by Ziegler-Biersack theory is probably restricted to a certain range of energy and dose of ions. The inadequacy of this approximation for higher energies was reported in [11].

The double-crystal topographs exhibit interference fringes in the implanted area. The distance between fringes in the topographs is dependent on the angular position in the rocking curve and they became more dense close to the peak [6]. These fringes are also more distinct in the topographs taken with synchrotron multicrystal arrangement. Two representative topographs of the sample implanted with protons are shown in Fig. 4. In the presently considered relatively flat samples the fringe formation is caused by inhomogeneous ion dose distribution: That was confirmed by the difference in the rocking curves taken from different regions which may be also observed in Fig. 1.

In some cases when the distribution of the ion dose was regular it was possible to reproduce the character of the fringes using a kind of column approximation. It is illustrated in Fig. 5 showing the comparison of photometric profile across the implanted area with a numerical simulation in 4.8 MeV α-particle implanted silicon. We assumed here the variation of the ion dose described by a top fragment of the Gaussian curve.

The synchrotron back-reflection section pattern representative for flat sample is shown in Fig. 6. This topograph is characteristic for more sensitive reflection with higher indices. We may notice the strong line corresponding to the entrance of the beam into the sample and a complicated pattern corresponding to the vicinity of the buried layer. In this region a characteristic sequence of three black strips is seen. The first black strip (second from the top in the topograph) which is usually wide and intense is expected to be the direct contrast coming from the region with a significant lattice parameter gradient. The following clear gap is due to the mostly deformed region similarly as in the topographic image of dislocations. The following second black strip comes from the rear side of the buried layer where the lattice parameter is again decreasing. The last strip is due to the reflection from the bulk and the prior clear gap is probably due a possible kind of secondary extinction due to the reflection from the top layer.

The position of the direct contrast due to the buried layer can be used for direct determination of its location below the surface. As may be easily found the distance t_f on the section pattern for an arbitrary spot is related to the corresponding depth t_s by the following formula:

$$t_s = t_f \frac{\cos(\alpha_h)\sin(\Theta-\varphi)}{\sin(2\Theta+\alpha_h)} = t_f A_h \qquad (7)$$

where: Θ denotes as previously the Bragg-angle for centrally adjusted reflection, φ denotes the inclination of the reflecting planes for centrally adjusted reflection and α denotes the angle between the projection of reflected beam of considered reflection on the vertical plane and the direction of reflected beam of centrally adjusted reflection. The values of α_h can be calculated from the position of spots on the film. The adequate accuracy of the evaluation requires exact knowledge of the entrance angle of the beam with respect to the surface and the misorientation of the planes with respect to the surface. A realistic value of 0.25° of accuracy, provides usually 5% of accuracy in determination of ranges.

The evaluated values of ion ranges were 21 μm for 4.8 MeV α-particles, 18 μm for 1 MeV protons and 36 μm for 1.6 MeV protons. These values are in good agreement with those based on Monte Carlo calculations from [12].

The character of the Bragg-case section pattern was well reproduced using the numerical integration of the Takagi-Taupin equations at it is shown in Fig. 7.

In some of the recorded patterns we observed characteristic interference tails shown in fig. 8a. They appear when the change of ion dose along the beam intersecting the sample takes place. It may be expected that they are due to the interference of the radiation reflected from the bulk and the radiation reflected from the rear region of the shot-through layer. The interference tails were revealed in simulated images assuming a variation of ion dose along the beam as is representatively shown in fig. 8b. Similarly as the periodicity of interference maxima in double-crystal rocking curves the periodicity of the fringes strongly depended on the phase factor due to the vertical displacement of the shot-through layer p. A reasonable agreement was obtained also assuming validity of eq.(5).

The character of Bragg-case section pattern both in the implanted and non-implanted areas is drastically changed when the crystal is elastically bent. In this case additional distinct interference fringes may be observed in the regions of a few millimetres behind the system of stripes discussed previously. In the case of bent substrates this phenomena was discussed in [13-15] and good approximation of interference patterns were obtained by numerical integration of the Takagi-Taupin equations.

In the case of implanted region the interference pattern is much more complicate and containing several systems of fringes as is shown in Fig. 9. The character of this picture was to some extend reproduced in numerical simulation shown in fig. 10. In this case we assumed a two dimensional variation of the ion dose

$$N(x,y) \approx \exp\left(\frac{ax^2+y^2}{2\sigma^2}\right) \qquad (8)$$

where x and y are the surface coordinates. In addition in some cases the sharp edges of implanted area were introduced using a rough approximation

$$\Delta N(x,y) = 0, \qquad \text{for } bx^2+y^2 \geq r_c \qquad (9)$$

where the value r_c was chosen to position the boundary inside the area of integration and a and b are the coefficients controlling the extension along the x co-ordinate. Similarly as in previous calculations the vertical incoherence of the crystal lattice was taken into account. Some discrepancies between the experimental and theoretical images come from more irregular character of ion dose distribution. In actual case the radius of curvature was close to 100 m.

Conclusions

The silicon implanted with high energy light ions was studied by means of various X-ray methods realized using conventional and synchrotron radiation sources. In most cases the characteristic rocking curves with increasing period of the subsidiary maxima for lower angles of incidence were obtained The double crystal topographs revealed interference fringes with the period also increasing for lower angles.

In the case of flat samples the back-reflection synchrotron section topography produced a series of stripes corresponding to the reflection from the surface and the vicinity of the buried layer. The location of these stripes enables the evaluation of the depth of different layers and the evaluation of ion ranges. The bending of the samples introduced additional wide spread interference pattern extended up to few millimetres behind the entrance of the beam.

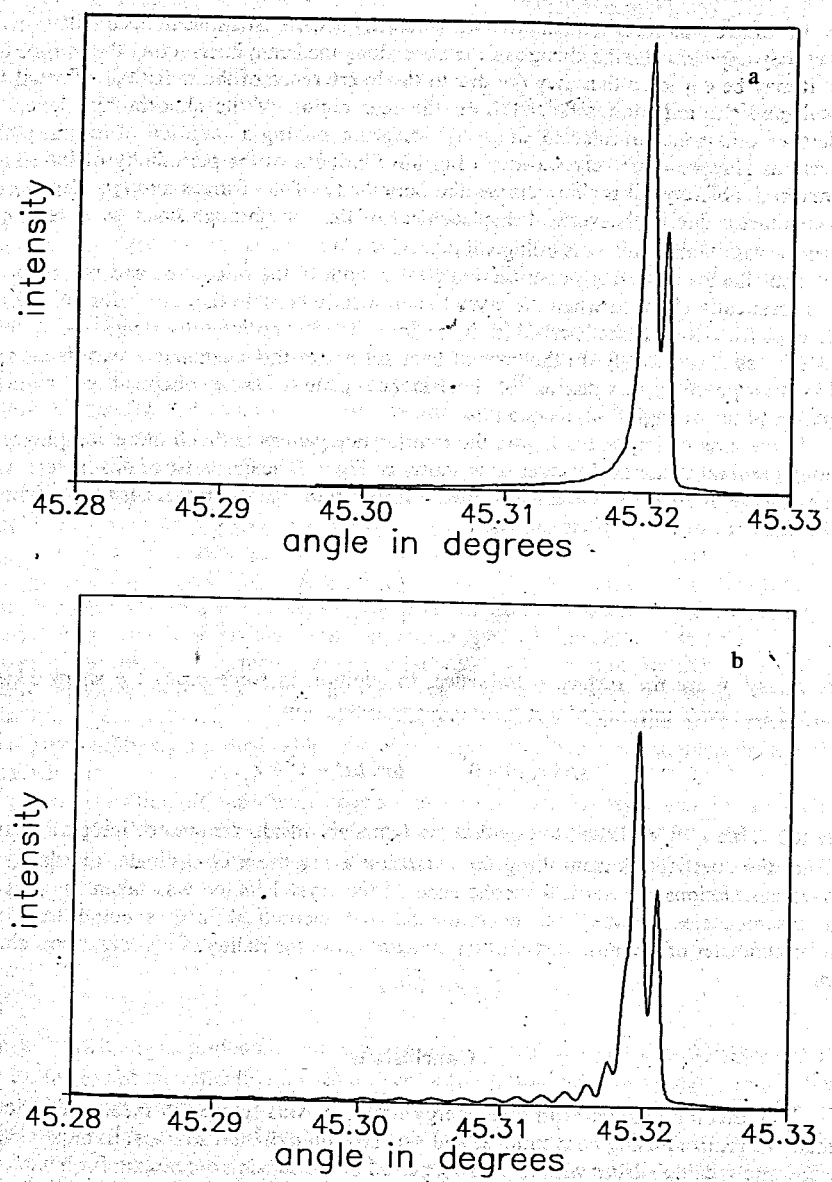

Fig. 1
Two experimental rocking curves for the 1 MeV proton implanted silicon taken with synchrotron triple-crystal arrangement with symmetrical 333 reflection of 1.35 Å wavelength. The curves were recorded from 0.1 × 0.1 mm^2 areas of the implanted region differing in the ion dose. The ion dose is lower in the case of the curve *a*.

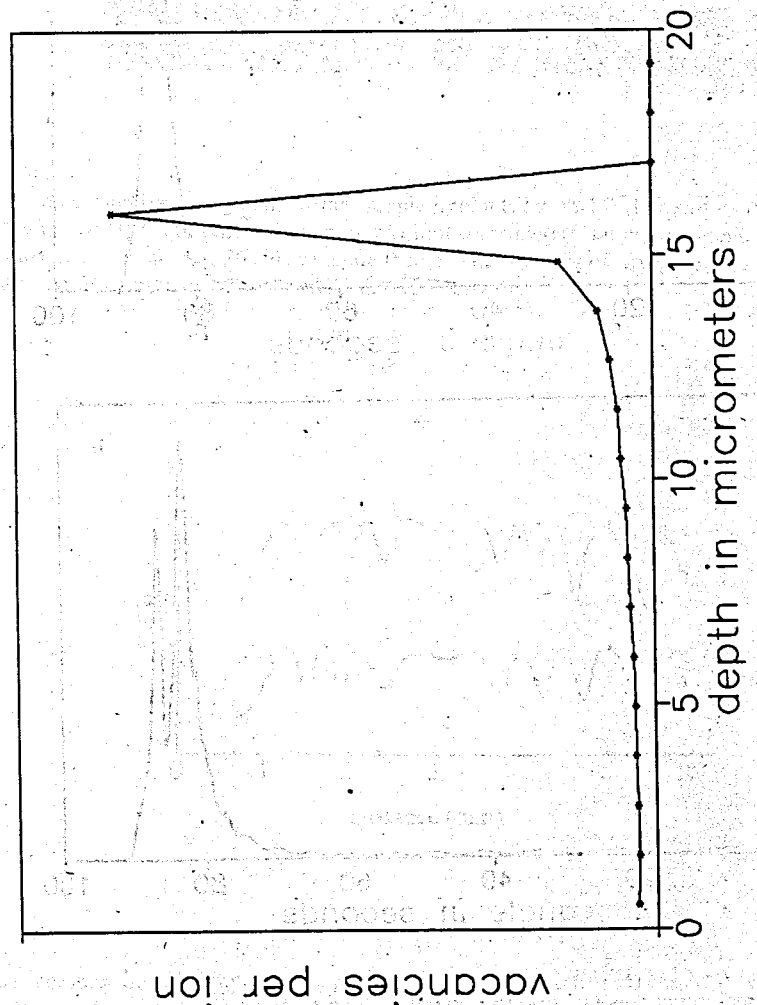

Fig. 2
The distribution of vacancies (expected to be accompanied by interstitials) obtained using TRIM-85 program for presently studied silicon implanted with 1 MeV protons.

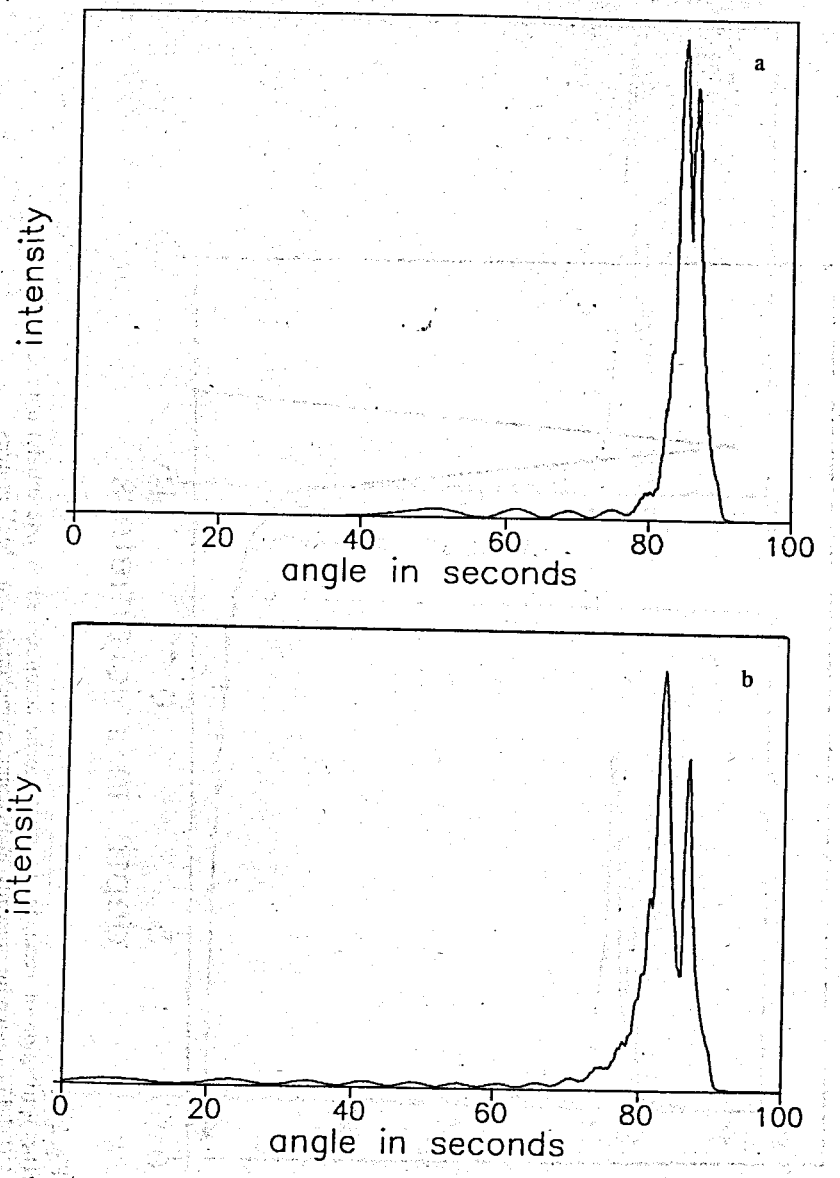

Fig. 3
The convoluted rocking curves taking into account 0.5" probe beam divergence obtained by numerical integration of Takagi-Taupin equation in 333 reflection of 1.35 Å wavelength assuming the lattice parameter depth profile proportional to that shown in Fig. 2. The curve *a* corresponds to 2 × lower ion dose than curve *b*.

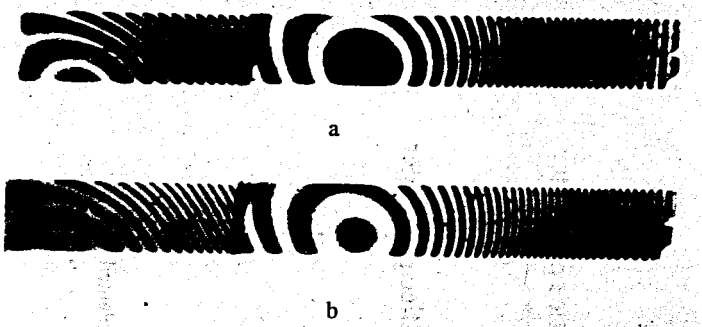

Fig. 4
Two representative topographs of the sample implanted with 1.6 (left part of the picture) and 1 MeV protons (right part) taken with synchrotron triple-crystal arrangement. The topograph shown in *a* was taken at 26" lower angle than *b*. The numbers of fringes in the area implanted with 1 MeV energy are 31 in *a* and 33 in *b* respectively.

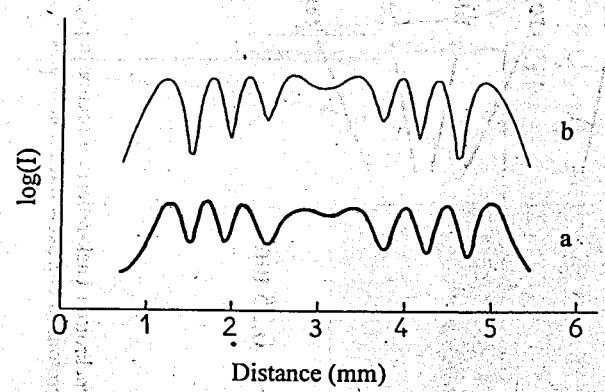

Fig. 5
The comparison of photometric profile across the implanted area (*a*) with numerical simulation (*b*) in 4.8 MeV α-particle implanted silicon. The simulation was obtained assuming the variation of the ion dose described by a top fragment of the Gaussian curve.

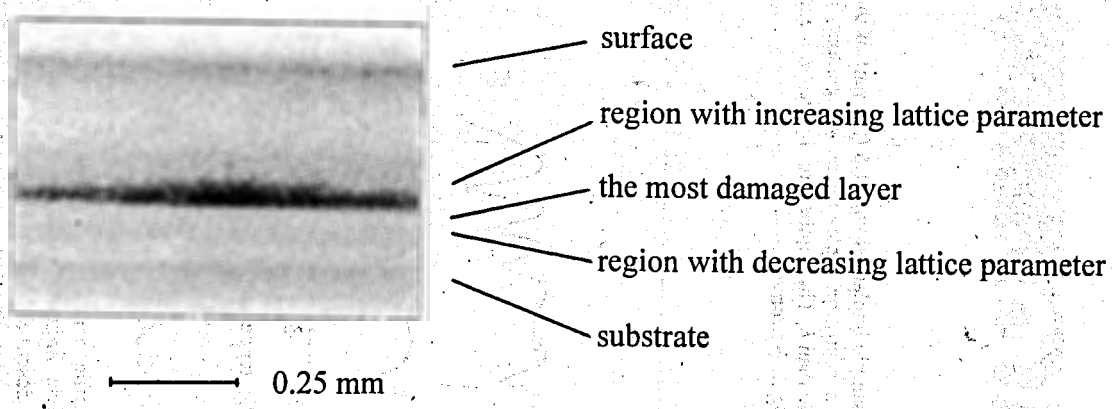

Fig. 6
White beam synchrotron back-reflection section topograph of flat silicon crystal implanted with 1.6 MeV protons in 642 skew reflection of 0.61 Å wavelength.

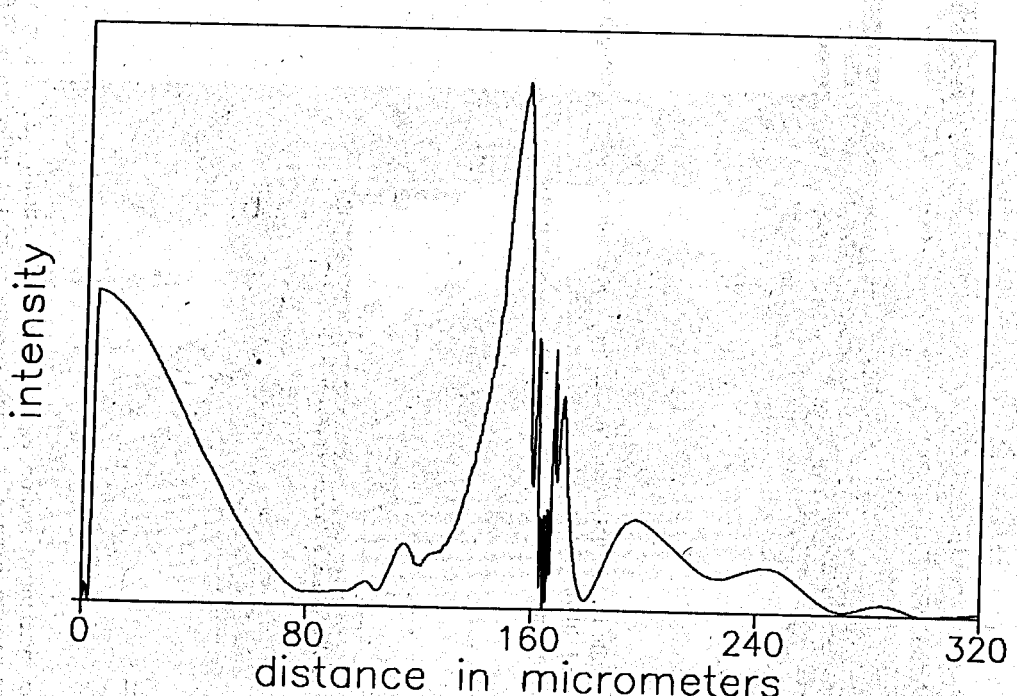

Fig. 7
Numerical simulation of intensity distribution for synchrotron section topograph in 553 reflection of 0.4 Å wavelength, assuming the lattice parameter depth distribution profile coming from Biersack-Ziegler theory.

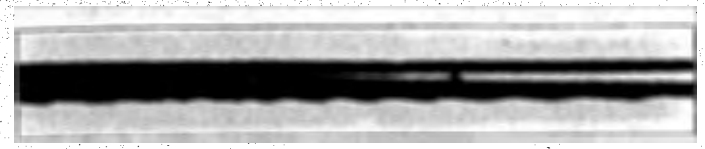

a

b

Fig. 8
a - The interference tails in 131 back-reflection section topograph in 1 Å wavelength of 1 MeV protons implanted silicon crystal.
b - The simulation of the interference fringes similar to those shown in *a*.

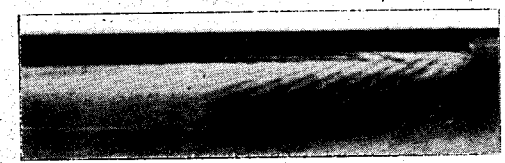

Fig. 9
The back-reflection synchrotron section topograph of the elastically bent silicon wafer implanted with non-uniform beam of 4.1 MeV α-particles in 111 reflection of 0.66 Å radiation.

Fig. 10
The representative two-dimensional numerical simulation of Bragg-case section pattern of implanted silicon bent wafer for 533 reflection of 0.37 Å radiation. The distribution of ion dose is described by two-dimensional Gaussian distribution with the tails cut off along the elliptical contour.

It was possible to obtain reasonable approximation of most of these results by numerical integration of the Takagi-Taupin equations. The lattice parameter profiles corresponding to the vacancy-interstitial distribution obtained using Biersack-Ziegler TRIM-85 program was assumed. A proportional factor, including the ion dose, was used as a fitting parameter and the incoherence of lattice due to vertical displacement was taken into account.

References

[1] U. Bonse, M. Hart and G.H. Schwuttke: *phys. stat. sol.* (a) **33**, 361 (1969).

[2] A.G. Serdakyan, V.S. Haroutyunyan, P.H. Bezirganyan, M. Subotowicz and G.K Trouni: *phys. stat. sol.* (a) **123**, 83 (1991).

[3] R.N. Kyutt, P.V. Petrashen and M. Sobokin: *phys. stat. sol.* (a) **60**, 381 (1980).

[4] M. Fatemi, P.E. Thompson and J. Chaudhuri: *J. Appl. Phys.* **68**, 3694 (1990).

[5] K. Wieteska, W. Wierzchowski: *phys. stat. sol.* (a) **147**, 55 (1995).

[6] K. Wieteska: *phys. stat. sol.* (a) **68**, 179 (1981).

[7] K. Wieteska, W. Wierzchowski: submitted to *J. Appl. Cryst.*

[8] T. Bedyńska: *phys. stat. sol.* (a) **18**, 57 (1973).

[9] J.F. Ziegler, J.P. Biersack and U. Littmark: *The Stopping and Range of Ions in Solids* ed. J.F. Ziegler Pergamon Press 1985.

[10] E. Estop, A. Izrael and M. Sauvage: *Acta Cryst.* A**32**, 627 (1976).

[11] J.N. Górecka and J. Auleytner: *phys. stat. sol.* (a) **137**, 309 (1993).

[12] J. Tatarkiewicz: *phys. stat. sol.* (a) **63**, 423 (1980).

[13] I. J. Shulpina, P. V. Petrashen, F. N. Chukhowskii and K. T. Gabrielyan: Tezisi Dokl. IV Vsesoyuz. Soveth. Defecti Strukturi w Poluprovodnikach, Novosibirsk 23-25 Oktyabr 1984, part 2, p. 114 (In Russian).

[14] J. Bąk-Misiuk, J. Gronkowski, J. Härtwig and W. Wierzchowski: *phys. stat. sol.* (a) **99**, 345 (1987).

[15] F. N. Chukhovski, P. V. Petrashen: *Acta Cryst.* A**44**, 8 (1988).

Received by Publishing Department
on May 29, 1996.